

SYNTHETIC IMAGES OF BLOOD MICROCIRCULATION TO ASSESS PRECISION OF VELOCITY PROFILES BY A CROSS-CORRELATION METHOD

Marianne Fenech, Boris Chayer, Guy Cloutier

Laboratory of Biorheology and Medical Ultrasonics, University of Montreal Hospital Research Center, Montreal, Quebec, Canada

ABSTRACT

Optical cross-correlation methods have been used to study the motion of red blood cells (RBC) in the microcirculation. To evaluate the precision of such a method to determine RBC velocity profiles, we developed a computational model of the microscopy image formation. The following steps were undertaken: 1) a mechanical model was used to mimic three dimensional RBC movements in a tubular parabolic flow; 2) at each time step, a synthetic image was built using microscopic image formation equations based on the depth of correlation of RBCs; and 3) the velocity profile was extracted by a cross-correlation algorithm applied to these synthetic images. The estimated maximum velocities extracted from the simulated images were always smaller than velocities found by simulation. Relative errors (4% to 25%) depended on the vessel radius and on the shape of the velocity profile, but not on the hematocrit or on the maximum velocity.

Index Terms— Mechanical modeling, red blood cells, maximum velocity, velocity profile, microscopic particle image velocimetry.

1. INTRODUCTION

The two-dimensional cross-correlation method is often used to study the red blood cell (RBC) microcirculation in vitro and in vivo (with and without addition of microparticles) [1-4]. However, to measure velocities of only particles in the focal plane, as in microscopic particle image velocimetry (μ PIV), some recommendations have to be followed: the particle volume concentration should be less than 0.1%, and the particle diameter should be below 1 μ m [5, 6]. These recommendations are not applicable for blood cells, because the RBC largest diameter is approximately 7 μ m and the hematocrit (volume concentration) is approximately between 20% (in the microcirculation) and 50% (in the systemic circulation). Consequently, all RBCs present typically in a microvessel of 15 μ m in radius are visible and measured velocities are biased because they correspond to a weighted average of cell velocities both in and out of the focal plane.

To describe this phenomenon, the depth of correlation (*DOC*) is defined as the minimal distance that separates a particle from the image plane without affecting the picture [6]:

$$DOC = \frac{1}{2} \left[\frac{(1 - \sqrt{\varepsilon})}{\sqrt{\varepsilon}} \left(\frac{n^2}{NA^2} - 1 \right) \left(d_p^2 + \frac{1.49(M+1)^2 \lambda^2}{M^2 NA^2} \right) \right] \quad (1)$$

with ε the distance from the object plane beyond which the contribution becomes insignificant (we can empirically set ε to a value of 10% [6]), n is the index of refraction of the immersion medium between the microfluid and the lens ($n = 1.33$ for water), $\lambda = 0.6 \mu$ m is the wavelength of light, NA is the numerical aperture of the lens, d_p is the particle diameter, and M the magnification. Equation (1) gives a depth of correlation of 14 μ m for a RBC with $d_p = 7 \mu$ m, when it is observed with a lens characterized by $M = 40X$ and $NA = 0.8$. This confirms that all RBCs present in a typical microvessel of 15 μ m radius are visible and can affect the assessment of velocity profiles.

To circumvent the above issue, some researchers used particle tracking methods but to see individual cells, they had to dilute blood to non-physiological hematocrits [7-8]. Suggi et al. [2] used vessels with a diameter around 100 μ m, i.e. larger than a microvessel. Lima et al. [9] added fluorescent micro-particles to RBCs, but although the above mentioned μ PIV recommendations concerning the volume concentration of added particles and their size were respected, they had to dilute blood to non-physiological hematocrits to see fluorescent micro-particles. Bitsch et al. [3], to minimize effects of out-of-focus particles, proposed to use a so-called base-clipping technique. A specific grayscale threshold level was chosen and gray-scale values below this level were discarded. This approach seems attractive because it is possible to work under physiological conditions; however, its performance has not yet been assessed.

According to the above review, the goal of this study was to determine errors on velocity profiles measured by cross-correlation from movies of simulated flowing RBCs. Knowing ground true velocities by simulations, it became possible to assess such errors.

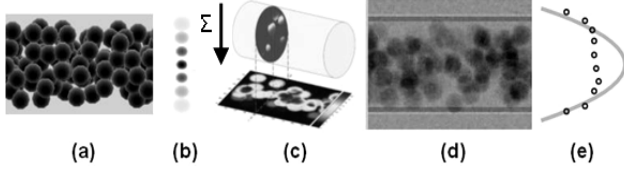


Figure 1: (a) 3D RBC flow from the mechanical model, (b) particle light and size depending on position (c) image formation by projection, (d) a synthetic image obtained, and (e) dots representing the mean velocity profile of RBCs from a series of synthetic images with the cross-correlation algorithm. The full line in (e) represents the real velocity profile of RBCs in (a).

2. METHODS

A computational model of the microscopy image formation was developed. This section presents the mechanical model that was used to mimic three dimensional (3D) RBC movements in a tubular parabolic flow, the strategy utilized to produce synthetic images, and the cross-correlation algorithm used to measure velocity profiles. Figure 1 summarizes these different steps.

2.1. Mechanical modeling of 3D RBC motions

Blood was considered as a collection of spheres interacting with each other and with the wall. The mechanical 2D modeling in [10] was extended to 3D to mimic real RBC movements in a tubular parabolic flow. The acceleration of a particle i over time t was given by:

$$m_i \frac{d\mathbf{v}_i}{dt} = \sum_{i \neq j} \mathbf{f}_{ij}^e + \mathbf{f}_{iw}^e + \mathbf{f}_i^h \quad (2)$$

where m_i is the mass of the particle i , \mathbf{v}_i is its velocity, \mathbf{f}_{ij}^e represents the force of the particle j acting on particle i , \mathbf{f}_{iw}^e is the force induced by the wall W on i , and \mathbf{f}_i^h is the hydrodynamic force. The hydrodynamic force \mathbf{f}_i^h induced by the Stokes drag on a sphere, assuming spherical isolated solid particles, with very small Reynolds and Stokes numbers (respectively < 1 and < 0.005), was given by :

$$\mathbf{f}_i^h = 6\pi\mu a (v_i^0 \mathbf{e}_i^0 - \mathbf{v}_i) \quad (3)$$

where μ is the dynamic viscosity of the fluid, a is the radius of the particle, \mathbf{v}_i is the current particle velocity, and $v_i^0 \mathbf{e}_i^0$ denotes the velocity of the fluid in the absence of particles, which drives the particle i to flow along the direction \mathbf{e}_i^0 at a speed of v_i^0 . To simulate a parabolic or flat velocity profile, the drive velocity was defined as follow:

$$v_i^0 \mathbf{e}_i^0 = V_{max} (1 - (r/R)^k) \mathbf{x} \quad (4)$$

where \mathbf{x} is the flow direction, r is the radial coordinate, R the radius of the vessel and V_{max} the maximum centerline

velocity. Note that $k = 2$ defines a parabolic profile and $k > 2$ a blunted profile. The elastic force was to exempt overlapping of RBCs. This force was inspired by a granular interaction model [11] and is given by:

$$\mathbf{f}_{ij}^e = K_E (2R - d_{ij})^{3/2} \mathbf{n}_{ij} \quad \text{if } d_{ij} < 2a \quad (5)$$

$$= 0 \quad \text{otherwise}$$

where K_E is the elasticity coefficient, d_{ij} represents the distance between centers of mass of RBCs i and j , and \mathbf{n}_{ij} is the normalized vector pointing from RBC j to i . Equation (5) shows that this force tends to repel RBCs when the distance between their centers of mass is smaller than the cell diameter. In the same way, the force between particles i and the wall was calculated as:

$$\mathbf{f}_{iw}^e = K_E (R - d_{iw})^{3/2} \mathbf{n}_{iw} \quad \text{if } d_{iw} < a \quad (6)$$

$$= 0 \quad \text{otherwise}$$

RBCs were modeled as spheres of radius $a = 2.8 \mu\text{m}$ to mimic the true volume of an erythrocyte and their mass m was 9.8×10^{-14} kg. Particles were initially positioned randomly without overlap in the 3D space. Using a finite difference scheme, velocities and positions of particles at time $t + dt$ were deduced from the acceleration at instant t according to Eq. (2). The time step was adapted at each iteration to obtain a maximal displacement of $0.05 \mu\text{m}$ for all RBCs. This method offered a good compromise between the stability of the numerical results and the computation time.

2.2. Synthetic images

Mechanical simulations gave RBCs' positions as a function of time. From these positions at each time-step (2000 images per second as in [12]), we simulated a 2D magnified image using microscopy image formation equations that consider shadowing and illumination effects.

2.2.1. Shadowing effect

The effective diameter (d_e) of an out of focus RBC (due to shadowing) shifted of a distance z from the object plane was approximated by [5] :

$$d_e(z) = \left[M^2 d_p^2 \frac{1.49(M+1)^2 \lambda^2}{M^2 NA^2} + \frac{M^2 D_a^2 z^2}{(s_0^2 + z^2)^2} \right] \quad (7)$$

where the magnification $M = 40 \times$, the numerical aperture of the lens $NA = 0.8$, the wavelength of light $\lambda = 0.6 \mu\text{m}$, the particle diameter $d_p = 5.6 \mu\text{m}$, the object distance $s_0 = 3.6 \text{mm}$, and the lens aperture diameter $D_a = s_0 / (2 \times NA)$.

2.2.2. Illumination effect

The total light flux from a single particle was modeled as 0 if it is in an empty zone and as $I(z) / Nv$ if the voxel is located in a RBC. Nv is the number of voxels that discretizes the RBC and $I(z)$ is given by Eq. (8):

$$I(z) = \frac{J_p D_a^2 \beta^2}{4\pi d_c^2 (s_0 + z)^2} \exp\left(\frac{-4\beta^2 a^2}{d_c^2} z\right) \quad (8)$$

with J_p the flux of light from the particule that was here equal to 1, $\beta = \sqrt{3.67}$ is the parameter of the gaussian distribution of the light intensity [5], and $a = d_p / 2$ is the RBC radius. The 3D space was discretized in voxels of $0.42 \times 0.42 \times 0.42 \mu\text{m}$ to fit images obtained with the experimental set-up of [12]. The 2D image was obtained by summing weights of all voxels following direction z . Finally, the matrix was normalized by applying a linear transformation to have the same maximum intensity as in the experimental pictures in [12], and, as CIMOS sensor noise can blur the contrast information in the picture, a noise level equivalent to that of the actual digital camera was added.

2.3 Computation of velocity profiles

The cross-correlation algorithm used in Chayer's in vitro study [12] was applied to determine velocity vectors from synthetic images. The size of the first correlation window was set to 15×15 pixels, and the size of the second interrogation window was of 60×60 pixels. An overlap of 100% minus one pixel was used. A median filter was employed to reject spurious vectors and a temporal filter was applied using 50 successive synthetic images with the hypothesis that the velocities were stabilized and stationary [12]. To increase the precision of the cross-correlation algorithm, the time between 2 successive images was chosen to get a displacement at the center of the vessel of at least three pixels. Here, this time was calculated with the known maximum velocity simulated by the mechanical model.

2.4. Simulation parameters

In the following, velocities obtained from mechanical simulations are designated with the superscript m and estimated velocities computed from simulated images with

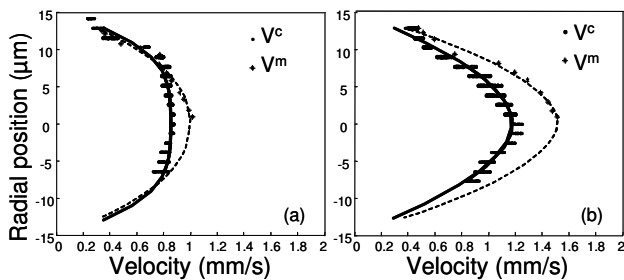


Figure 2: Estimated velocity profiles computed from simulated images with the cross-correlation method (V^c) and simulated velocity profiles (V^m) for two maximum velocities. Polynomial regressions using Eq. 4 were done to determine V_{max}^m , V_{max}^c , k^m and k^c . Dotted lines show the regression of the data from mechanical simulation, and the continuous line that of the data computed from simulated images. The hematocrit was 20%, the vessel radius $15 \mu\text{m}$ and $k = 2$.

the cross-correlation method are labeled with superscript c . RBC displacements were simulated for hematocrits of 20 and 40%, in vessels of $15 \mu\text{m}$ and $20 \mu\text{m}$ radii, with a sharp velocity profile ($k = 1.5$), a parabolic profile ($k = 2$) and a blunted profile ($k = 3$). For each case (same radius, same hematocrit, same k), the maximum velocity V_{max} was incremented from 0.1 mm/s to 2 mm/s . Velocity profiles were fitted using equation (4) to determine maximum velocities V_{max}^m and V_{max}^c and shape parameters k^m and k^c . Note that V_{max}^m and k^m could be slightly different (less than 5%) from V_{max} and k entered in equation (4) since the mechanical model accounts for RBC interactions due to collisions between neighboring cells.

3. RESULTS

3.1. Effect of changing the maximum velocity and hematocrit

Figures (2a) and (2b) show examples of estimated velocity profiles computed from simulated images with the cross-correlation method at different maximum velocities. V_{max}^c were always smaller than velocities imposed by simulation V_{max}^m . In figure (3), relative errors of the maximum velocity were computed as $(V_{max}^m - V_{max}^c) / V_{max}^m$.

As noted in figure (3a), underestimations of V_{max}^c versus V_{max}^m were amplified as the maximum velocity was increased. But the relative error appeared to be independent of V_{max}^c (Figure 3b). In addition, relative errors on V_{max}^c were bounded between 12% and 20%, approximately, for a parabolic velocity profile in a $15 \mu\text{m}$ vessel radius at 20% hematocrit. As seen in Tables 1 and 2, relative errors reached 25% for a sharp velocity profile ($k = 1.5$) in a vessel of $15 \mu\text{m}$, but it decreased to 4% for a flat profile in a vessel of $20 \mu\text{m}$. Changing the hematocrit from 20% to 40% did not significantly affect those errors on V_{max}^c .

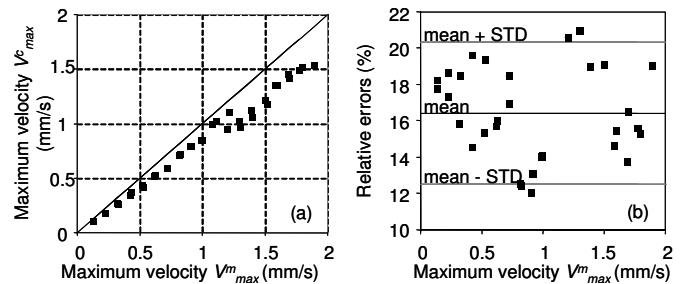


Figure 3: (a) V_{max}^c versus V_{max}^m . (b) Relative errors on the maximum velocity V_{max}^c versus V_{max}^m . Results for a hematocrit of 20%, a vessel radius of $15 \mu\text{m}$ and $k^m = 2$.

Table 1: Mean relative errors and standard deviations of the maximum velocity V_{max}^c for a hematocrit of 20 %, for three different velocity profiles and for two vessel radii.

$k \backslash$ Vessel radius	1.5	2	3
15 μm	23.9% \pm 4.3%	16.1% \pm 4.1%	9.3% \pm 2.4%
20 μm	13.4% \pm 4.2%	7.1% \pm 2.8%	4.0% \pm 4.2%

3.2 Effect of changing the shape of the velocity profile and vessel size

Tables 1 and 2 also pointed out a clear effect of k and of the vessel size on V_{max}^c relative errors. The shape of the velocity profile under physiological conditions is known to depend on the RBC aggregation level and hemodynamic conditions such as vessel curvature, entrance length, etc... [7]. According to these tables, relative errors on V_{max}^c were reduced for more blunted velocity profiles and for a larger diameter tube.

4. DISCUSSION

For the first time, the error on estimated velocity profiles of flowing RBCs visualized in microscopy and computed with a cross-correlation method was evaluated. V_{max}^c were always smaller than V_{max}^m , the relative error was found to depend on the vessel radius and on the shape of the velocity profile, but not on the hematocrit or on the maximum velocity. Velocities computed by cross-correlation were affected by the optical system because they are a weighted average of cell velocities, in and out of the focal plane. As it was highlighted in this study, this averaging effect can be very important when velocities cover a large interval of values in the vessel transverse plane (case of small vessels with sharp velocity profiles).

Any cross-correlation method must be used with caution to study microcirculatory blood flow, especially for very small vessels. Our results were obtained under well defined conditions but nevertheless, they represent guidelines for microcirculatory optical studies. To conclude, it should be noted that optical theories on particle image formation have been formulated for the measurement of small, weakly concentrated particles. Our model can certainly be improved with a more accurate description of the image formation by considering theories on light ray propagation in matter. Also, future advancements in the domain of mechanical modeling of flowing RBCs should be profitable, especially to take into account the RBC biconcave shape and the RBC deformation in the microcirculation. Finally, the base-clipping technique to minimize effects of out-of-focus particles should be attempted and quantified.

Table 2: Mean relative errors and standard deviations of the maximum velocity V_{max}^c for a hematocrit of 40 %, for three different velocity profiles and for two vessel radii.

$k \backslash$ Vessel radius	1.5	2	3
15 μm	25.0% \pm 5.2%	15.4% \pm 2.9%	11.0% \pm 2.4%
20 μm	13.9% \pm 4.5%	6.8% \pm 3.5%	4.2% \pm 2.6%

ACKNOWLEDGMENTS

This work was jointly supported by grants from the NIH (#R01HL078655), CIHR (#CMI 72323) and HSFC (#PG-05-0313), and by a National Scientist Award of FRSQ. We are indebted to the RQCHP for the generous allocation of computer resources and to Dr. H. Ward for English proofreading.

REFERENCES

- [1] K. Tsukada, H. Minamitani, et al., *Image correlation method for measuring blood flow velocity in microcirculation: correlation 'window' simulation and in vivo image analysis*. *Physiol. Meas.* 2, pp. 459-471, 2000.
- [2] Y. Sugii, R. Okuda, et al., *Velocity measurement of both red blood cells and plasma of in vitro blood flow using high-speed micro PIV technique*, *Meas. Sci. Technol.* 16, pp. 1126-1130, 2005.
- [3] L. Bitsch, L.H. Olesen, et al., *Micro particle-image velocimetry of bead suspensions and blood flows*, *Exp. Fluid* 39, pp. 505-511, 2005.
- [4] A.G Koutsiaris and A. Pogiatz. *Velocity pulse measurements in the mesenteric arterioles of rabbits*. *Physiol. Meas.* 25, pp. 15-25, 2004.
- [5] M.G. Olsen and R.J. Adrian, *Out-of-focus effects on particle image visibility and correlation in microscopic particle image velocimetry*, *Exp. in Fluids* 29, pp. 166-174, 2000.
- [6] C.D. Meinhart, *Volume illumination for two-dimensional particle image velocimetry*, *Meas. Sci. Technol.* 11, pp. 809-814, 2000.
- [7] J.J. Bishop, A. S. Popel, et al., *Rheological effects of red blood cells aggregation in the venous network: a review of recent studies*, *Biorheology* 38, pp. 263-274, 2001.
- [8] S. Kim, A.S. Popel, et al., *Aggregate formation of erythrocytes in postcapillary venules*, *Am. J. Physiol. heart circ. Physiol.* 288, pp. 584-590, 2005.
- [9] R. Lima, *Confocal micro-piv measurements of three-dimensional profiles of cell suspension flow in a square microchannel*, *Meas. Sci. Technol* 17, pp. 797-808, 2006.
- [10] M. Fenech, D. Garcia et al., *A particle model of red blood cell aggregation kinetics*, submitted, 2008.
- [11] J. Duran, *Modélisations numériques. In Sables, poudres et grains: introduction à la physique des milieux granulaires*, Eyrolles sciences, Paris, pp. 215-226, 1997.
- [12] B.Chayer, J.A. de Guise and G. Cloutier. *Effect of depth of correlation on cross-correlation blood flow measurements in glass microchannels*, in press, ISBI 2008.